

Condensed matter physics of a strongly coupled gauge theory with quarks: some novel features of the phase diagram

Thomas Faulkner and Hong Liu

*Center for Theoretical Physics,
Massachusetts Institute of Technology,
Cambridge, MA 02139*

Abstract

We revisit the phase diagram of the $\mathcal{N} = 4$ $SU(N_c)$ super-Yang-Mills theory coupled to N_f fundamental “quarks” at strong coupling using the gauge-gravity correspondence. We show that in the plane of temperature v.s. baryon chemical potential there is a critical line of third order phase transition which ends at a tricritical point after which the transition becomes first order. Close to the critical line there is an intriguing logarithmic behavior, which cannot follow from a mean field type of analysis. We argue that on the string theory side the third order phase transition is driven by the condensation of worldsheet instantons and that this transition might become a smooth crossover at finite 't Hooft coupling.

I. INTRODUCTION

Fascinating new dynamical phenomena can appear when the coupling(s) of a system becomes strong. Familiar examples include color confinement and dynamical chiral symmetry breaking in QCD and high T_c superconductivity in various condensed matter systems. Yet strongly coupled systems are hard to solve and intuitions gained from weakly coupled systems normally do not apply.

The AdS/CFT correspondence [1] has provided important tools for studying many strongly coupled systems by relating them to classical gravity (or string) systems. A remarkable feature of the duality is that highly dynamical, strongly coupled phenomena in gauge theories can often be understood on the gravity side using simple intuitive geometric pictures. For example, confinement is reflected in the fact that a fundamental string, which represents an unbounded quark in the boundary gauge theory, has no place to end in the bulk geometry and thus cannot exist. New strongly coupled phenomena may be waiting to be discovered, and AdS/CFT maybe just the tool needed to discover it.

In this paper we are interested in understanding the phase structure of a large N_c gauge theory coupled to a small number N_f fundamental quarks at strong coupling from gravity. More precisely, we consider $\mathcal{N} = 4$ SYM theory with a gauge group $SU(N_c)$ coupled to N_f ($\mathcal{N} = 2$) hypermultiplets in the fundamental representation of $SU(N_c)$, which in the limit of $N_c \gg N_f$ and strong 't Hooft coupling can be described in terms of N_f probe D7-branes in the $AdS_5 \times S_5$ geometry [2]¹. Comparing to QCD, the system has the following distinct features:

1. $N_c \gg N_f$, while in QCD $N_c \sim N_f$.
2. There are both fermionic and *bosonic* “quarks”, which are charged under a $U(1)_B$ baryon number symmetry.
3. The beta-function for gauge coupling is zero to leading order in N_f/N_c . The scale of the system is set by the quark mass m_q .

Despite many important differences from QCD, the system appears to be rather interesting in its own right and provides a nice laboratory for studying strongly coupled quark-gluon

¹ See [3] for a review of the system.

systems under extreme conditions. At zero baryon density and finite temperature it has been used to model heavy quark mesons in QCD [4, 5]. At finite baryon density and zero temperatures some novel dynamical features were recently found in [6].

The phase diagram of the system at finite temperature T and baryon chemical potential² μ_q can be worked out by studying possible configurations of D7-branes in the background geometry (which is a black hole in $\text{AdS}_5 \times S^5$) and has been studied by various authors in [7–14]³. The results can be summarized as follows (see Fig. 1):

1. There is a transition curve in the $\mu_q - T$ plane which intersects with the horizontal axis at $\mu_q = m_q$ with m_q the bare quark mass, and with the vertical axis at some temperature $T = T_d$. Except for a small region near the vertical axis, the transition curve is given by

$$\mu_q = m_q^{(T)}(T) \tag{1}$$

where $m_q^{(T)}$ is the effective quark mass at finite temperature (it decreases with temperature).⁴ In particular, the transition is second order [11] along the horizontal axis ($T = 0$) and first order along the vertical axis ($\mu_q = 0$) [7]. The transition along the vertical axis at $T = T_d$ has been interpreted as a dissociation transition for mesons [7, 19, 20].

2. The region inside the curve in the $\mu_q - T$ plane is described by a D7-brane embedding which lies entirely outside the black hole (Minkowski-type embedding), while the region outside the curve is described by a configuration in which part of the D7-branes falls into the black hole (black hole-type embedding). In terms of the boundary gauge theory, the baryon number density is zero inside the curve and becomes nonzero outside (except along the vertical axis μ_q where the baryon density is always zero.)

In this paper we improve on the above description and show that the transition along the curve (1) is a *continuous* (3rd order) phase transition which connects to a first order line

² In this paper we will use the terms baryon charge density and quark charge density interchangeably without a factor $1/N_c$ between them. In other words we take the $U(1)_B$ charge of a quark (anti-quark) to be 1(-1).

³ For related studies of the same system see [15–17] and for related studies of a confining theory see [18]

⁴ For a precise definition of $m_q^{(T)}$ see discussion around eqs. (12)–(14) in sec. II A.

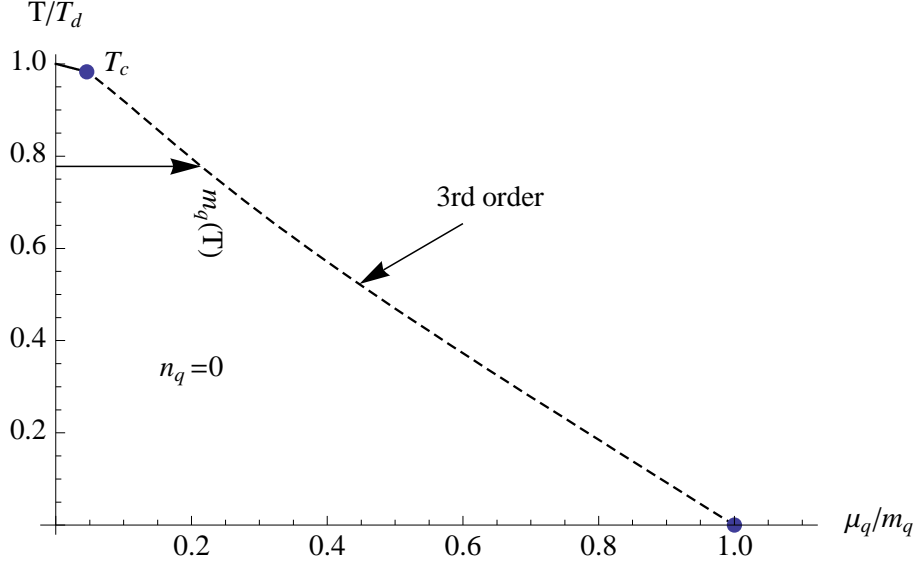


FIG. 1: The phase diagram in the $\mu_q - T$ plane. The dashed line indicates a continuous transition. The transition line lies exactly on the curve $m_q^{(T)}$ until a critical temperature T_c very close (but not equal) to the dissociation temperature T_d .

(near the vertical axis) through a tricritical point whose location we identify precisely, see Fig .1.

While our conclusions of a continuous phase transition along (1) are consistent with the analysis of [10] who noted a phase transition along the $m_q^{(T)}$ line at zero density they are different from a later discussion in [12] where a first order transition was noted. In [12] the relation between charge density and temperature was studied numerically near the transition line and a very small discontinuity in density was noticed, due to a change in dominance between a Minkowski type embedding with zero density and a black hole embedding. It appears to us that the discontinuity likely has to do with the numerical accuracy of their calculation. We do not find a discontinuity in charge density along the transition line (see equation (2) below)⁵. More importantly, we have identified a clear physical reason for the phase transition, which indicates that it should not be considered as an exchange of dominance between different embedding solutions, which was behind the reasoning of the conclusion in [12]. As observed in [21], for Minkowski type embedding at finite temperature, there are worldsheet instanton corrections to the leading order Dirac-Born-Infeld (DBI) ac-

⁵ We have obtained our results both analytically and numerically with agreement.

tion for the D7-branes. While for a Minkowski type embedding, particle excitations on the D7-branes are not sensitive to the value of the chemical potential, the worldsheet instantons which correspond to semi-classical strings stretched between D7-branes and the black hole do. In particular, when the baryon chemical potential exceeds the value (1), the instanton actions exponentially dominate over the DBI action in the large 't Hooft coupling limit and induce an instability. The consequence of the instability is that instantons “condense” and generate a genuine neck between the D7-branes and the black hole. Thus beyond (1) the Minkowski-type embedding cannot exist and should be replaced by a black hole type embedding.⁶ The transition also has a simple interpretation in the gauge theory. As discussed in [21], the instantons can be interpreted in boundary gauge theory as thermal medium quarks. When μ_q exceeds the value of (1), the quarks have negative free energies and will condense and generate a finite charge density, although it is not clear whether it is fermionic quarks or bosonic quarks which are condensing.

More explicitly, we find along the critical line (1) (approaching it from above), the baryon charge density and the chemical potential are related by

$$\mu_q - m_q^{(T)} = -B(T)\epsilon \log \epsilon + A(T)\epsilon + O(\epsilon^2) \quad (2)$$

where ϵ is the quark charge density (normalized to be dimensionless) and $A(T), B(T)$ are some functions of temperature. In the zero temperature limit, $B(T)$ goes to zero and $A(T)$ goes to a finite constant, and one recovers the second transition at $T = 0$ (found in [11]), where various exponents are given by their mean field values. At any finite temperature, however, it is always the logarithmic term on RHS of (2) that dominates at small enough densities and as a result the transition becomes third order. The logarithmic behavior does not appear to have a mean field counterpart, and thus this is an example of continuous phase transition from gravity which does not obey the Landau-Ginsburg behavior. Such log terms however do appear to be a common feature of the renormalization group analysis of condensed matter systems at their upper critical dimension.

There also exists a temperature T_c at which $B(T_c) = 0$ and beyond which $B(T) < 0$. At

⁶ Note that this reasoning does not by itself imply that the transition should be continuous, it only indicates that the transition is not an exchange of dominance as is normally the case for a first order transition. Our explicit calculation shows that there is no jump in the baryon charge density across the transition line in the infinite 't Hooft coupling limit.

T_c the transition is again second order. For $T > T_c$, the transition becomes first order since for a given μ_q close to, but *smaller* than $m_q^{(T)}$, now there are two black hole type embeddings with $\epsilon \neq 0$ in addition to the Minkowski type embedding. Connecting a continuous critical line and a first order transition line, the point $(T = T_c, \mu_q = m_q^{(T)}(T_c))$ is thus a tricritical point. Again the critical behavior near the tricritical point is *not* the same as that of a Landau-Ginsburg type effective theory.

While it is natural to connect the first transition near the tricritical point with that near the vertical axis at $\mu_q = 0$, our approximation in (2) which applies to small densities does not extend all the way to $\mu_q = 0$. Thus that part of the phase diagram remains a conjecture at the moment. Also numerical work at *finite* density by other authors [12] suggest this should be the case, however a conclusive argument remains to be made.

The phase diagram in Fig. 1 is for the $\lambda = \infty$ limit, where the quark charge density is identically zero inside the transition curve. At finite λ , as pointed out in [21], for any $\mu_q \neq 0$ at any finite temperature, the baryon charge density is in fact nonzero, given by a dilute Boltzmann gas of quarks. This immediately raises the question whether the transition along (1) is an artifact of the infinite λ limit and will be smoothed into a crossover at any finite λ . To settle this question requires summing over the worldsheet instantons found in [21] and will be pursued in a separate publication.

The plan of the paper is as follows. In section II we discuss the gravity description of the gauge theory system. In sec II A we review the general gravity setup for describing $\mathcal{N} = 4$ SYM theory coupled to N_f fundamental hypermultiplets at finite temperature. In sec. II B we review how to introduce a finite baryon chemical potential. In sec. II C we argue that the phase transition is driven by string worldsheet instantons. In sec III we give a detailed analytically derivation of equation (2) and verify it numerically. In sec. IV we discuss the thermodynamics of the system which can be gathered from equation (2). In the conclusion sec. V we discuss the connection of the critical point to the first order dissociation transition at $\mu_q = 0$. We also discuss what happens to the phase diagram at finite λ .

II. GRAVITY DESCRIPTION OF THE GAUGE THEORY

A. General set-up

At finite temperature, $\mathcal{N} = 4$ SYM theory with a gauge group $SU(N_c)$ can be described by a string theory in the spacetime of a black hole in $\text{AdS}_5 \times S_5$, whose metric can be written as

$$ds^2 = \frac{r^2}{R^2} (-f dt^2 + d\vec{x}^2) + \frac{R^2}{r^2} \frac{dr^2}{f} + R^2 d\Omega_5^2 \quad (3)$$

where $\vec{x} = (x_1, x_2, x_3)$ and

$$f = 1 - \frac{r_0^4}{r^4}. \quad (4)$$

$d\Omega_5^2$ is the metric on a unit five-sphere S_5 . The string coupling g_s and the curvature radius R (in units of α') are related to the Yang-Mills coupling g_{YM} and N_c by

$$4\pi g_s = g_{YM}^2, \quad \frac{R^2}{\alpha'} = \sqrt{\lambda}, \quad \lambda = g_{YM}^2 N_c. \quad (5)$$

The temperature T of the YM theory is given by the Hawking temperature of the black hole,

$$T = \frac{r_0}{\pi R^2}. \quad (6)$$

One can introduce “quarks” to the system by adding to $\mathcal{N} = 4$ SYM theory N_f $\mathcal{N} = 2$ hypermultiplets in the fundamental representation of the gauge group. In the limit of large N_c with N_f finite this can be described in the dual string theory side by adding N_f D7-branes in the black hole geometry (3) and to leading order in N_f/N_c , the backreaction of the D7-branes on the background geometry can be neglected. A fundamental “quark” in the YM theory can be described by an open string with one end on the D7-branes and the other end on the black hole. Strings corresponding to quarks and anti-quarks have opposite orientations. Open strings with both ends on the D7-branes can be considered as “bound states” of a quark and antiquark, thus describing meson-type excitations in the YM theory.

In the limit

$$N_c \rightarrow \infty, \quad \lambda \rightarrow \infty, \quad N_f = \text{finite} \quad (7)$$

which corresponds to the limit $g_s \rightarrow 0$, $\frac{\alpha'}{R^2} \rightarrow 0$ in the string theory side, the geometric embedding and the dynamics of the D7-branes can be described using the Dirac-Born-Infeld (DBI) action

$$S = -N_f T_7 \int d^8 \xi \sqrt{-\det(g_{mn} + 2\pi\alpha' F_{mn})}. \quad (8)$$

where g_{mn} denotes the induced metric on the D7-brane and $T_7 = \frac{1}{(2\pi)^7 g_s \alpha'^4}$ is the tension of a D7-brane. This will be the limit we work with for most of the paper. We will also consider in the discussion section what happens when one relaxes the $\lambda = \infty$ limit, where new interesting physics could emerge.

To describe the embedding of the D7-branes in (3), it is more convenient to introduce a new radial coordinate u defined by

$$\frac{dr^2}{r^2 f(r)} = \frac{du^2}{u^2}, \quad \implies \quad r^2(u) = \frac{u^4 + u_0^4}{u^2} \quad \text{with} \quad u_0 \equiv \frac{r_0}{\sqrt{2}} \quad (9)$$

in terms of which (3) can be written as

$$\begin{aligned} ds^2 &= -\frac{r^2(u)}{R^2} f(u) dt^2 + \frac{r^2(u)}{R^2} d\vec{x}^2 + \frac{R^2}{u^2} (du^2 + u^2 d\Omega_5^2) \\ &= \frac{u^2}{R^2} q(u) (-f dt^2 + d\vec{x}^2) + \frac{R^2}{u^2} (d\rho^2 + \rho^2 d\Omega_3^2 + dy^2 + y^2 d\phi^2) \end{aligned} \quad (10)$$

where

$$u^2 = y^2 + \rho^2, \quad f(u) = \frac{(u^4 - u_0^4)^2}{(u^4 + u_0^4)^2}, \quad q(u) \equiv \frac{r^2(u)}{u^2} = 1 + \frac{u_0^4}{u^4}. \quad (11)$$

In (10), we have split the last term of the first line in terms of polar coordinates on $\mathbb{R}^4 \times \mathbb{R}^2$ with $d\Omega_3^2$ denoting the metric on a unit three-sphere. The D7-branes can be chosen to lie along the directions $\xi^\alpha = (t, \vec{x}, \Omega_3, \rho)$ and using the symmetries of the problem the embedding in the two remaining transverse directions can be taken as $\phi(\xi^\alpha) = 0$ and $y(\xi^\alpha) = y(\rho)$. $y(\rho)$ can be found by solving the equation of motion obtained from the DBI action (8) with the boundary condition

$$y(\infty) = L = (2\pi\alpha') m_q \quad (12)$$

where m_q can be interpreted as the (bare) mass of the ‘‘quarks’’. We denote the resulting embedding function as $y_0(\rho)$, which were first obtained numerically in [13]. At a small temperature, the brane lies entirely outside the black hole, as indicated schematically in Fig. 2. The brane is closest to the black hole at $\rho = 0$, where the three-sphere in last term of (10) shrinks to a point. Denoting

$$y_0(\rho = 0) = L_0 \quad (13)$$

then the shortest open string connecting the D7-brane to the horizon has a mass in the YM theory

$$m_q^{(T)} = \frac{1}{2\pi\alpha'} \int_{u_0}^{L_0} dy \sqrt{fq} \Big|_{\rho=0}. \quad (14)$$

$m_q^{(T)}$ can be interpreted as the effective mass of the “quarks” at temperature T . Note that $m_q^{(T)}$ decreases monotonically with T , since as we increase the temperature, the black hole becomes bigger and gravity attracts the brane more to the black hole. There exists a temperature $T_d (= 2.166m_q/\sqrt{\lambda})$, after which the branes fall into the black hole (often called black hole embedding) through a first order phase transition [7, 20]. We will be interested in the temperature range smaller or of order T_d in which regime we always have ($\beta = \frac{1}{T}$)

$$\beta m_q^{(T)} \sim O(\sqrt{\lambda}) . \quad (15)$$

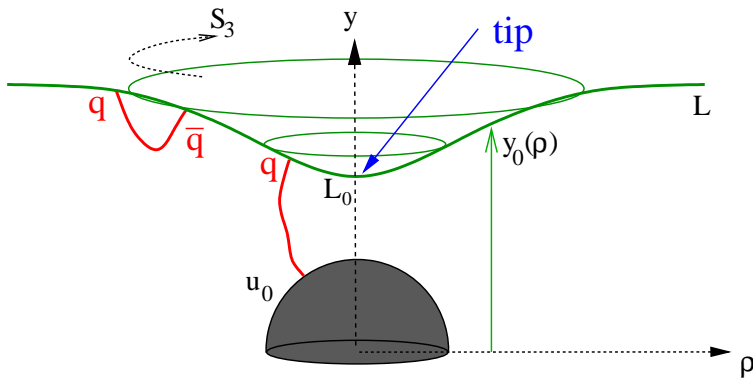


FIG. 2: An embedding of the D7 brane (green) in the $AdS_5 \times S_5$ black hole geometry which lies entirely outside the black hole. The exact form of the embedding has been exaggerated to emphasize certain features.

B. Finite baryon chemical potential

The system possesses a $U(1)_B$ global baryon symmetry under which “quarks” transform nontrivially. The associated conserved current J_B^μ is dual to the $U(1)$ gauge field A_μ on the D7-branes. Turning on a chemical potential μ_q for the charge density in the boundary theory then corresponds to imposing the following boundary condition⁷ for A_μ

$$A_0(\rho = \infty) = \mu_q . \quad (16)$$

The charged density n_q can be calculated from the bulk theory by

$$n_q = \Pi^0(\rho = \infty) \quad (17)$$

⁷ Also, if the D7-branes fall into the horizon there will also be a boundary condition that $A_0 = 0$ at the horizon.

where Π^0 is the canonical momentum conjugate to A_0 (in terms of ρ -slicing) evaluated at the classical solution which satisfies the boundary conditions (12) and (16). Again by symmetry we will take A_0 to depend only on ρ and the other components of the gauge field will be set to zero.

The DBI action (8) can be written explicitly in terms of $y(\rho), A_0(\rho)$ as

$$S = -N_f T_7 \int d^8 \xi \rho^3 q^{3/2} [f q (1 + (y')^2) - a'^2]^{\frac{1}{2}}, \quad (18)$$

where prime denotes derivative with respect to ρ , and we have introduced

$$a(\rho) = 2\pi\alpha' A_0. \quad (19)$$

We will denote the integrand of (18) as \mathcal{L} . Since (18) does not depend on a (only a') we have a conserved quantity ϵ :

$$\epsilon = \frac{\partial \mathcal{L}}{\partial a'} = \frac{a' \rho^3 q^{3/2}}{(f q (1 + (y')^2) - a'^2)^{\frac{1}{2}}} \quad (20)$$

$$a'^2 = f q (1 + y'^2) \frac{\epsilon^2}{\rho^6 q^3 + \epsilon^2}. \quad (21)$$

From (17), we thus find the charge density in the boundary gauge theory is given by

$$n_q = N_f T_7 (2\pi\alpha') (2\pi^2) \epsilon \quad (22)$$

where the factor $2\pi^2$ comes from the volume of the three sphere.

Since we will be expanding in terms of small density later, it will be convenient to scale coordinates and ϵ so that they are dimensionless, i.e.

$$u, y, \rho \rightarrow L_0(u, y, \rho), \quad \epsilon \rightarrow L_0^3 \epsilon, \quad a(\rho) \rightarrow L_0 a(\rho) \quad (23)$$

where L_0 is the location of the tip of the brane (13) *before* turning on a chemical potential⁸.

From now on, $u, y, \rho, \epsilon, a(\rho)$ are all dimensionless. After the scaling (11) become

$$u^2 = y^2 + \rho^2, \quad q(u) \equiv 1 + \frac{\eta^4}{u^4}, \quad f \equiv \left(\frac{u^4 - \eta^4}{u^4 + \eta^4} \right)^2, \quad \eta \equiv \frac{u_0}{L_0} < 1. \quad (24)$$

⁸ One can also choose to normalize them using L (12) which is more directly related to the field theory mass. But in our calculation below using L_0 is slightly more convenient. L_0 is fixed once the ratio m_q/T is given. Another alternative is to use the temperature but that will make the zero temperature limit more subtle.

The boundary conditions for $y(\rho)$ and $a(\rho)$ now are

$$y(\infty) = \frac{L}{L_0}, \quad a(\infty) = \frac{2\pi\alpha'}{L_0}\mu_q \quad (25)$$

and equation (14) becomes

$$m_q^{(T)} = \frac{L_0}{2\pi\alpha'} \int_{\eta}^1 dy \sqrt{fq} \Big|_{\rho=0} . T \quad (26)$$

To obtain the equation of motion for y it is convenient to perform a Legendre transformation on (18) to express it in terms of ϵ . The transformed action is

$$\mathcal{H} \equiv \epsilon a' + \mathcal{L} = \sqrt{\epsilon^2 + \rho^6 q^3} \sqrt{fq(1 + y'^2)} \quad (27)$$

which leads to equation of motion

$$\frac{y''}{1 + y'^2} + \frac{3y'}{\rho} + \frac{8}{u^2} \frac{\rho y' - y}{u^8 \eta^{-8} - 1} - \frac{\epsilon^2}{\epsilon^2 + \rho^6 q^3} \left[\frac{3y'}{\rho} - \frac{6}{u^2} \frac{\rho y' - y}{1 + u^4 \eta^{-4}} \right] = 0 . \quad (28)$$

When $\epsilon = 0$ (i.e. zero density), equation (28) becomes

$$\frac{y''}{1 + y'^2} + \frac{3y'}{\rho} + \frac{8}{u^2} \frac{\rho y' - y}{u^8 \eta^{-8} - 1} = 0 \quad (29)$$

whose solution is given by $y_0(\rho)$ described earlier around equation (13).⁹ In Fig. 3 we plot how L_0/L and η change with temperature for an embedding governed by $y_0(\rho)$.

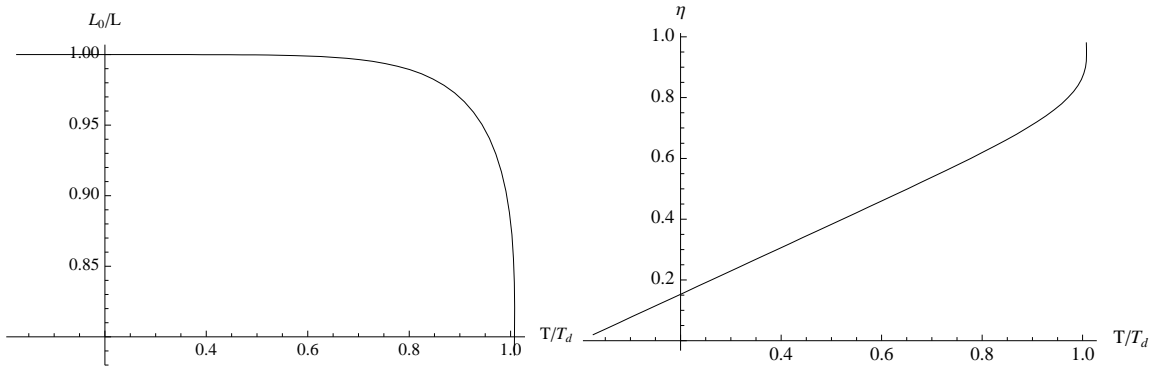


FIG. 3: L_0/L and η for the Minkowski solution ($\epsilon = 0$) as a function of T/T_d .

⁹ As stated earlier we will only consider $T < T_d$ for which there is only one Minkowski embedding solution.

C. Phase transition driven by string worldsheet instantons

For *any* value of μ_q (and $T < T_d$), one can always have the following solution to equations of motion (21) and (28) with

$$A_0 = \mu_q = \text{const}, \quad \epsilon = 0, \quad y(\rho) = y_0(\rho) \quad (30)$$

for which (28) reduces to (29). This solution is somewhat peculiar, since it implies that the quark charge density n_q is zero even at a finite temperature and finite chemical potential μ_q . This appears to contradict with field theory expectation that the density for quark and anti-quark should be given (at low density) by the Boltzmann distribution $n_{\pm} \sim e^{-\beta(m_q^{(T)} \pm \mu_q)}$ which gives a nonzero net charge density $n_q = n_+ - n_- \neq 0$ for a nonzero μ_q . There is in fact no contradiction, since (30) is the result in the $\lambda = \infty$ limit (supergravity limit) and in this limit due to (15),

$$n_{\pm} \sim n_q \sim e^{-\sqrt{\lambda}}, \quad \text{for } \mu_q < m_q^{(T)}. \quad (31)$$

The charge density is thus exponentially small in the large λ limit and not visible to any order in the $1/\sqrt{\lambda}$ (or α') expansion.

In [21], it was found for the embedding (30) there are non-perturbative open string worldsheet instanton corrections to the DBI action (8) which accounts for the exponentially small quark density. More explicitly, the instantons are given by open strings stretching between the tip of the D7-branes and the black hole horizon and winding around the Euclidean time direction, as indicated in the left plot of Fig. 4. They are classified a winding number n . From the spacetime point of view, these instantons generate tiny virtual necks which connect the tip of the branes to the black hole horizon. The total Euclidean action for the D7-branes, which gives the thermodynamic potential of the boundary gauge theory in the grand canonical ensemble, can be written as

$$S = S_{DBI} + \sum_{n=\pm 1, \pm 2, \dots} D_n \exp(-|n|\beta(m_q^{(T)} - \text{sgn}[n]\mu_q)) + \dots \quad (32)$$

where n sums over the instanton contributions, D_n arises from the worldsheet determinant for each instanton¹⁰, and \dots denotes other perturbative $1/\sqrt{\lambda}$ (or α') corrections. These string worldsheet instantons have a simple interpretation in the boundary gauge theory as

¹⁰ It also includes possible integrations over instanton moduli space.

representing thermal medium quarks. In particular, the $n = \pm 1$ terms in (32) are precisely what one expects of a dilute Boltzmann gas of quarks and anti-quarks.¹¹

Due to (15), when $\mu_q < m_q^{(T)}$ the instanton contributions in (32) are exponentially small in $\sqrt{\lambda}$ compared with the DBI action S_{DBI} . But for

$$\mu_q \geq m_q^{(T)} \tag{33}$$

the instanton sum will be exponentially large compared with the DBI action and the solution (30) can no longer be trusted. In particular, since the instanton contributions are dominating, we expect them to “condense” and create a genuine neck between the brane and the black hole. This implies in the range (33) a new solution to the DBI action with the branes going into the black hole should emerge, as indicated in the right plot of Fig. 4. Thus in the infinite λ limit we have a phase transition at $\mu_q = m_q^{(T)}$ where the Minkowski-type embedding (30) goes over to a black-hole-type embedding. The transition also has a simple interpretation from the gauge theory point of view; when μ_q satisfies (33), the quarks have negative free energies and will thus condense and generate a finite charge density.

The possibility for such a phase transition has been studied before in [9, 10, 12], where a single¹² black hole embedding solution was found for $\mu_q > m_q^{(T)}$ and it was concluded in [12] that the transition was *first order*. One reason for the conclusion was that it appeared that the Minkowski embedding solution (30) was still valid for $\mu_q > m_q^{(T)}$ and thus the transition appeared to be a change of dominance between different solutions. As we discussed above, the Minkowski embedding solution should be *replaced* by a black hole embedding solution in the parameter region (33). Thus if there is only a single black hole embedding solution for $\mu_q > m_q^{(T)}$ the transition is most likely to be continuous. Indeed we will show in section IV, the transition is *third order* for temperature not too high, but then becomes first order through a *tricritical point*.¹³

¹¹ Higher n contributions should encode corrections due to Bose-Einstein or Fermi-Dirac statistics and other corrections due to interactions.

¹² at a temperature not too high

¹³ Beyond the tricritical point it becomes possible to have multiple black hole embedding solutions for a given μ_q . See section IV.

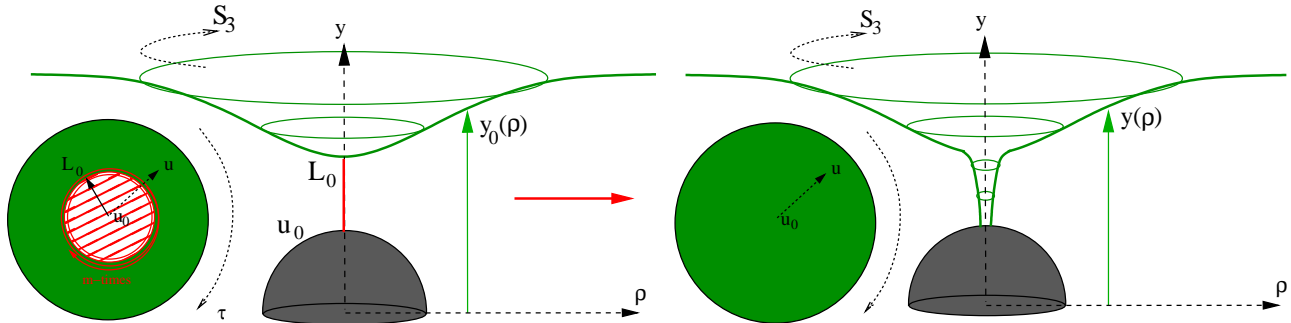


FIG. 4: Left plot: For Minkowski type embedding (30), there exist worldsheet instantons which correspond to semi-classical strings stretching between the tip of the D7-branes to the black hole horizon and winding around the Euclidean time direction represented as the angle on the inset disk. The radial direction on the disk is the same as the radial direction in the $y - \rho$ plane. Right plot: for $\mu_q > m_q^{(T)}$ instantons dominate over the DBI contributions and will condense to form a genuine neck between the branes and the horizon, i.e. one should have a black hole type embedding.

D. Black hole embedding at finite density

As discussed in last subsection, for $\mu_q \geq m_q^{(T)}$ we expect a black hole type embedding for D7-branes in the gravity side and a nonzero quark charge density on the gauge theory side. That the quark density for a black hole type embedding should be zero can be seen as follows. For a black hole type embedding, one should impose an additional boundary condition $A_0 = 0$ for the gauge field at the horizon in order to ensure the regularity of the solution. From (16) this implies that A_0 should evolve nontrivially from the boundary to the horizon, i.e. there is a nontrivial electric field in the radial direction on the branes, which from (17) in turn implies $n_q \neq 0$ (and thus $\epsilon \neq 0$). Thus we should now consider equation (28) with $\epsilon \neq 0$. Conversely it has also been argued previously in [16] that for any $\epsilon \neq 0$, only black hole type of embeddings are allowed since for a Minkowski type embedding it is not possible to have a non-singular distribution of a finite charge density on the branes¹⁴.

Let us now consider the boundary conditions for $y(\rho)$ at the horizon for a black hole type embedding. We will denote the point that the brane enters the horizon ρ_c and $y_c \equiv y(\rho_c)$. Note that

$$y_c^2 + \rho_c^2 = u_0^2 \quad (34)$$

¹⁴ See also [11] for a discussion at zero temperature

and in order for the the third term in (28) to be nonsingular at the horizon, we will also need that

$$y'(\rho_c) = \frac{y_c}{\rho_c} \quad (35)$$

i.e. the brane should be perpendicular to the horizon. The precise value of ρ_c is determined by the boundary condition (25).

For regularity we will also require the gauge potential vanish at the horizon¹⁵, i.e. $a(\rho_c) = 0$. From equation (21), we can express the chemical potential in terms of density ϵ as

$$\mu_q = \frac{L_0}{2\pi\alpha'} \epsilon \int_{\rho_c}^{\infty} d\rho \frac{\sqrt{fq(1+y'^2)}}{\sqrt{\epsilon^2 + \rho^6 q^3}}. \quad (36)$$

The main technical task of the paper is to determine the behavior of μ_q in the limit of small ϵ , which will be carried out in next section. Once the expansion of μ_q in terms of ϵ is known, we will be able to determine the order of the phase transition and other thermodynamic properties of the system. This will be carried out in section IV.

III. SMALL DENSITY EXPANSION OF THE CHEMICAL POTENTIAL

In this section we study the behavior of (36) in the small ϵ limit. Expanding (36) in small ϵ is somewhat complicated since the solution $y(\rho)$ depends nontrivially on ϵ . The expansion of $y(\rho)$ in terms of small ϵ is also involved; one cannot treat the ϵ -dependent term in (28) as a small perturbation of (29) uniformly for all values of ρ since the term becomes of $O(1)$ for sufficiently small ρ (when $\rho^6 q^3 \sim O(\epsilon^2)$).

The main result of the section is equation (60). Readers who are not interested in the detailed derivation can go directly to (60) and subsequent discussions.

A. Expansion of the solution

Since the perturbation in ϵ is not uniform in ρ one needs to divide the ρ axis into different regions, treating the perturbations in each region separately, and matching them together at the end. For our purpose, it turns out enough to split the ρ -axis into two regions:

- **Inner** $\rho = \epsilon^{\frac{1}{2}}\sigma$ for $\sigma_c < \sigma < \Lambda$

¹⁵ Otherwise the one-form $A_0 dt$ will be singular at the horizon since the norm for $\frac{\partial}{\partial t}$ vanishes there.

- **Outer** $\rho_\Lambda < \rho < \infty$

where

$$\rho_c = \epsilon^{\frac{1}{2}} \sigma_c, \quad \rho_\Lambda = \epsilon^{\frac{1}{2}} \Lambda . \quad (37)$$

The reason for the choice of scaling in the inner region can be seen by letting $\rho = \epsilon^\alpha \sigma$ in (28) and one finds that for $\epsilon = \frac{1}{2}$ a nontrivial scaling limit exists, which results differential equation in (44) below. Also see Appendix B for a discussion of the $T = 0$ solution where this scaling is evident.

We will consider the limit

$$\epsilon \rightarrow 0, \quad \sigma = \text{finite}, \quad \Lambda \rightarrow \infty, \quad \rho_\Lambda \rightarrow 0 . \quad (38)$$

We expand the solution in the inner and outer regions as¹⁶

$$y_{\mathcal{I}}(\sigma) = Y_0(\sigma) + \epsilon Y_1(\sigma) + \epsilon^2 Y_2(\sigma) + \dots \quad (39)$$

$$y_{\mathcal{O}}(\rho) = y_0(\rho) + \epsilon y_1(\rho) + \epsilon^2 y_2(\rho) + \dots . \quad (40)$$

Plugging (39) and (40) respectively into (28) and expanding the equation in ϵ , we obtain a series of differential equations for various functions in (39) and (40). These equations are rather complicated and not exactly solvable. We will work out the behavior of $Y_0(\sigma), Y_1(\sigma)$ in the large σ limit and $y_0(\rho), y_1(\rho)$ in the small ρ limit and match them in the overlapping region. Fortunately it turns out this is enough to find the leading expansion of μ_q in the small ϵ limit analytically.

Let us first examine the outer region. y_0 is simply the solution to (29) which describes the embedding at zero density. It satisfies the boundary condition (25) at the boundary and near $\rho = 0$ has the following expansion

$$y_0(\rho) = 1 + \frac{\rho^2}{\eta^{-8} - 1} - \frac{\eta^8(5 + 5\eta^8 - 3\eta^{16})}{3(1 - \eta^8)^3} \rho^4 + O(\rho^6) . \quad (41)$$

y_1 satisfies a homogeneous linear equation obtained by linearizing (29). For small ρ it has an expansion,

$$y_1 = b_{-1} \rho^{-2} + b_0 \log \rho + b_1 + O(\rho) \quad (42)$$

¹⁶ While it is not a priori obvious the expansion parameter should be ϵ and not some other power, the expansions below do yield consistent results.

where b_{-1} and b_1 are integration constants and

$$b_0 = -\frac{28\eta^8}{(1-\eta^4)^2(1+\eta^4)^2}b_{-1}. \quad (43)$$

Note that the first two terms diverge in the $\rho \rightarrow 0$ limit. The coefficient b_{-1} of the quadratically divergent term will be fixed later by matching with the inner solution. b_1 should be determined by requiring $y_1(\rho \rightarrow \infty) \rightarrow 0$ since y_0 already satisfies the required boundary condition (25) there.

Now we look at the inner region. $Y_0(\sigma)$ satisfies a second order *non-linear* differential equation (primes below denotes derivative w.r.t. σ)

$$\frac{Y_0''}{Y_0'^2} + 3 \left(1 + \frac{\eta^4}{Y_0^4}\right)^3 \sigma^5 Y_0' + \frac{8}{Y_0^2} \frac{\sigma Y_0' - Y_0}{Y_0^8 \eta^{-8} - 1} + \frac{6}{Y_0^2} \frac{\sigma Y_0' - Y_0}{1 + Y_0^4 \eta^{-4}} = 0 \quad (44)$$

From (34) and (35) the boundary condition at the horizon is

$$Y_0(\sigma_0) = \eta, \quad Y_0'(\sigma_0) = \frac{\eta}{\sigma_0} \quad (45)$$

where σ_0 is an integration constant. σ_0 is the zero-th order term in the expansion in ϵ of $\sigma_c = \rho_c/\epsilon^{1/2}$ (where again it is a non trivial fact that this expansion begins at $\mathcal{O}(1)$ in ϵ)

$$\sigma_c = \sigma_0 + \epsilon \sigma_1 + \dots \quad (46)$$

and can be determined by the boundary condition at infinity,

$$Y_0(\sigma) \rightarrow 1 \quad \text{as} \quad \sigma \rightarrow \infty. \quad (47)$$

The above condition is fixed by comparing with the leading term in (41). At large σ , Y_0 has the expansion

$$Y_0(\sigma) = 1 - \frac{1}{2(1+\eta^4)^{3/2}}\sigma^{-2} + \frac{\eta^4(-3+5\eta^4)}{4(-1+\eta^4)(1+\eta^4)^4}\sigma^{-4} + \frac{\eta^4(27-131\eta^4+153\eta^8-105\eta^{12})}{24(-1+\eta^4)^2(1+\eta^4)^{13/2}}\sigma^{-6} + O(\sigma^{-8}) + O(\sigma^{-8} \log \sigma) \quad (48)$$

Note that the coefficient before σ^{-8} is an integration constant which can be fixed by (45). We will not need its value below.

$Y_1(\sigma)$ satisfies a second order *linear* differential equation with coefficients that depend on $Y_0(\sigma)$. It is not homogeneous and rather complicated. We will not write it here. For large σ we find the expansion

$$Y_1(\sigma) = a_{-1}\sigma^2 + a_0 \log \sigma + a_1 + O(\sigma^{-1}) \quad (49)$$

where a_1 is an integration constant (the other integration constant presumably appears at higher order in the expansion) and

$$a_{-1} = \frac{\eta^8}{1 - \eta^8}, \quad a_0 = \frac{14\eta^8}{(1 - \eta^4)^2(1 + \eta^4)^{\frac{7}{2}}}. \quad (50)$$

Note the first two terms of (49) are divergent as $\sigma \rightarrow \infty$. The constant a_1 can be determined by matching with the solution of the outer region. The *other* boundary condition is determined by the regularity condition (34-35) (expanded to this order) at the horizon, this gives only one boundary condition on Y_1 and its derivative because the first order correction σ_1 in (46) is a free parameter. This parameter σ_1 would then be determined by the resulting solution.

We will now determine various integration constants above by matching the solutions in the inner and outer regions around ρ_Λ . Note given the relation $\rho = \epsilon^{\frac{1}{2}}\sigma$, the ϵ expansion in the outer region is reshuffled compared to that in the inner region. Comparing the first term in (42) to the second term of (48) we find that

$$b_{-1} = -\frac{1}{2(1 + \eta^4)^{3/2}}, \quad b_0 = \frac{14\eta^8}{(1 - \eta^4)^2(1 + \eta^4)^{\frac{7}{2}}} \quad (51)$$

where we have used (43) in obtaining the second equation. From (51) and (50) we see that the logarithmic term in (42) precisely match with that in (49); this is a nontrivial self-consistency check of our expansion. It now remains to match the constant terms in (42) and (49). Given the difference in the argument of logarithmic term in (42) and (49), we thus find that

$$a_1 = b_1 + \frac{1}{2}b_0 \log \epsilon = b_1 + \frac{7\eta^8}{(1 - \eta^4)^2(1 + \eta^4)^{\frac{7}{2}}} \log \epsilon. \quad (52)$$

As remarked below (43), b_1 is determined by the boundary condition $y_1(\infty) = 0$ and since the equation for y_1 is independent of ϵ , so is b_1 .¹⁷ Thus we see from (52) that the integration constant a_1 for inner solution Y_1 now contains a $\log \epsilon$ piece!¹⁸ This will be important in our determination of the leading order behavior for μ_q below.

As a check on our above results we can make sure that the exact (numerical) solution at small densities matches well onto our expansions in the two different regions. This is demonstrated in Fig. (5). The agreement is very precise suggesting the two regions we have

¹⁷ Determining b_1 requires solving the two-point boundary value problem for y_1 .

¹⁸ This in turn implies that σ_1 in (46) also contains $\log \epsilon$.

used are sufficient. Higher order corrections in the two regions would appear as divergences toward the exact solution.

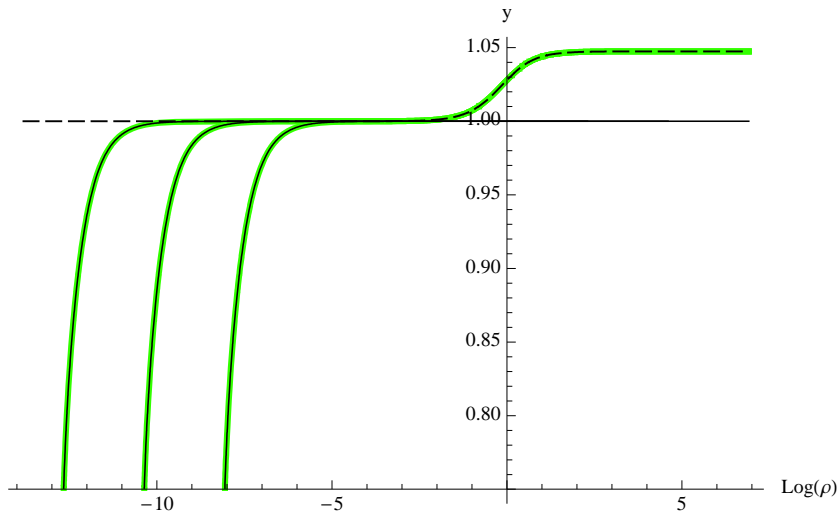


FIG. 5: The exact embeddings for $\epsilon = 10^{-11}, 10^{-9}, 10^{-7}$ shown in green. To clearly show the two regions we have plotted $y(\rho)$ as a function of $\log(\rho)$. These are compared to the zeroth order inner (*solid*) and outer (*dashed*) solutions. The inner solution $Y_0(\sigma)$ is a function of $\sigma = \rho\epsilon^{-1/2}$ so for the various fixed densities the curve is simply shifted along the $\log(\rho)$ axis. The agreement between the three curves on the overlapping regions is very precise.

B. Expansion of the chemical potential

We now look at the small ϵ expansion of (36). We will give the main steps and final results, leaving further details to Appendix B.

The μ_q integral (36) can be split into integrals over the inner and outer regions

$$\mu_q = \int_{\rho_c}^{\rho_\Lambda} (\dots) + \int_{\rho_\Lambda}^{\infty} (\dots) \equiv \mu_{\mathcal{I}} + \mu_{\mathcal{O}} . \quad (53)$$

$\mu_{\mathcal{I}}$ and $\mu_{\mathcal{O}}$ can now be expanded in terms of ϵ using (39) and (40). The outer region contribution $\mu_{\mathcal{O}}$ starts with order ϵ , i.e.

$$\mu_{\mathcal{O}} = \epsilon \mu_{\mathcal{O}}^{(1)} + O(\epsilon^2) \quad (54)$$

and for $\mu_{\mathcal{O}}^{(1)}$ only y_0 is needed. Using the small ρ expansion of y_0 (41) we find that the

integral for $\mu_{\mathcal{O}}^{(1)}$ contains a quadratic and a logarithmic divergent term in the limit $\rho_{\Lambda} \rightarrow 0$,

$$\mu_{\mathcal{O}}^{(1)} = \frac{L_0}{2\pi\alpha'} \left(\frac{1 - \eta^4}{2(1 + \eta^4)^2 \rho_{\Lambda}^2} - \frac{2\eta^4(3 - \eta^4 + 3\eta^8)}{(1 - \eta^4)(1 + \eta^4)^4} \log(\rho_{\Lambda}) + K_{\mathcal{O}}(\eta, L/L_0) \right) \quad (55)$$

where $K_{\mathcal{O}}$ denotes the part which remains finite in the limit $\rho_{\Lambda} \rightarrow 0$ $K_{\mathcal{O}}$, whose explicit expression is given in Appendix B, depends on the full solution $y_0(\rho)$ and can only be evaluated numerically.

The inner region contribution also contains an $O(1)$ piece

$$\mu_{\mathcal{I}} = \mu_{\mathcal{I}}^{(0)} + \epsilon \mu_{\mathcal{I}}^{(1)} + \dots \quad (56)$$

with (recall that $\sigma = \epsilon^{-\frac{1}{2}}\rho$)

$$\mu_{\mathcal{I}}^{(0)} = \frac{L_0}{2\pi\alpha'} \int_{\sigma_c}^{\Lambda} d\sigma Y_0'(\sigma) \frac{Y_0^4 - \eta^4}{Y_0^2 \sqrt{Y_0^4 + \eta^4}} = \int_{\sigma_c}^{\infty} (\dots) - \int_{\Lambda}^{\infty} (\dots) \quad (57)$$

where in the second equality we have separated the expression into two pieces by splitting the integral. Now changing the integration variable of the first integral into Y_0 and comparing it with (26), we find that it is precisely $m_q^{(T)}$. The second term can be evaluated in power series of $1/\Lambda$ by using the expression (48) for Y_0 at large σ , leading to

$$\mu_{\mathcal{I}}^{(0)} = m_q^{(T)} - \frac{L_0}{2\pi\alpha'} \frac{(1 - \eta^4)}{2(1 + \eta^4)^2 \Lambda^2} + \mathcal{O}(\Lambda^{-4}) . \quad (58)$$

To evaluate $\mu_{\mathcal{I}}^{(1)}$ one also needs Y_1 . Using the expansion (49) of Y_0 and Y_1 for large σ , we find that the integral for $\mu_{\mathcal{I}}^{(1)}$ contains a logarithmic divergence (in the $\Lambda \rightarrow \infty$ limit) from the upper end of the integral and can be written as

$$\mu_{\mathcal{I}}^{(1)} = \frac{L_0}{2\pi\alpha'} \left(\frac{2\eta^4(3 - \eta^4 + 3\eta^8)}{(1 - \eta^4)(1 + \eta^4)^4} \log(\Lambda) + \frac{7\eta^8 \log \epsilon}{(1 - \eta^4)(1 + \eta^4)^4} + K_{\mathcal{I}}(\eta, L/L_0) \right) . \quad (59)$$

Note that in the finite part we have isolated a piece proportional to $\log \epsilon$ which comes from the integration constant a_1 of Y_1 through equation (52) (see Appendix B for details). $K_{\mathcal{I}}$ is finite and independent of ϵ . Its explicit expression is given in B and can only be evaluated numerically.

Now adding (55) and (58), (59) together we find that the second term in (58) precisely cancels the quadratic divergence in (55) and the logarithmic divergence in (59) precisely cancels with that in (55), leaving a finite piece proportional to $\epsilon \log \epsilon$. We thus find that

$$\mu = m_q^{(T)} - B(T)\epsilon \log \epsilon + A(T)\epsilon + O(\epsilon^2) \quad (60)$$

where

$$B(T) = B_1(T) + B_2(T) = \frac{L_0}{2\pi\alpha'} \frac{\eta^4(3 - 8\eta^4 + 3\eta^8)}{(1 - \eta^4)(1 + \eta^4)^4}, \quad A(T) = \frac{L_0}{2\pi\alpha'} (K_{\mathcal{O}} + K_{\mathcal{I}}) \quad (61)$$

and

$$B_1(T) = \frac{L_0}{2\pi\alpha'} \frac{\eta^4(3 - \eta^4 + 3\eta^8)}{(1 - \eta^4)(1 + \eta^4)^4}, \quad B_2(T) = -\frac{L_0}{2\pi\alpha'} \frac{7\eta^8}{(1 - \eta^4)(1 + \eta^4)^4} \quad (62)$$

Note that in writing (61) and (62) we have emphasized that the coefficient of $\epsilon \log \epsilon$ receives contributions from two different sources; B_1 from cancellation of the logarithmic divergence and B_2 from the finite piece in (59). The expressions for $K_{\mathcal{O}}$ and $K_{\mathcal{I}}$ are given in Appendix B, which can only be evaluated numerically. We also note that in the $\epsilon \rightarrow 0$ limit it is the $\epsilon \log \epsilon$ which dominates and whose coefficient we have determined exactly. Note that L_0 , which gives of the location of the tip of the D7-branes in the absence of a charged density (13), is also temperature-dependent.

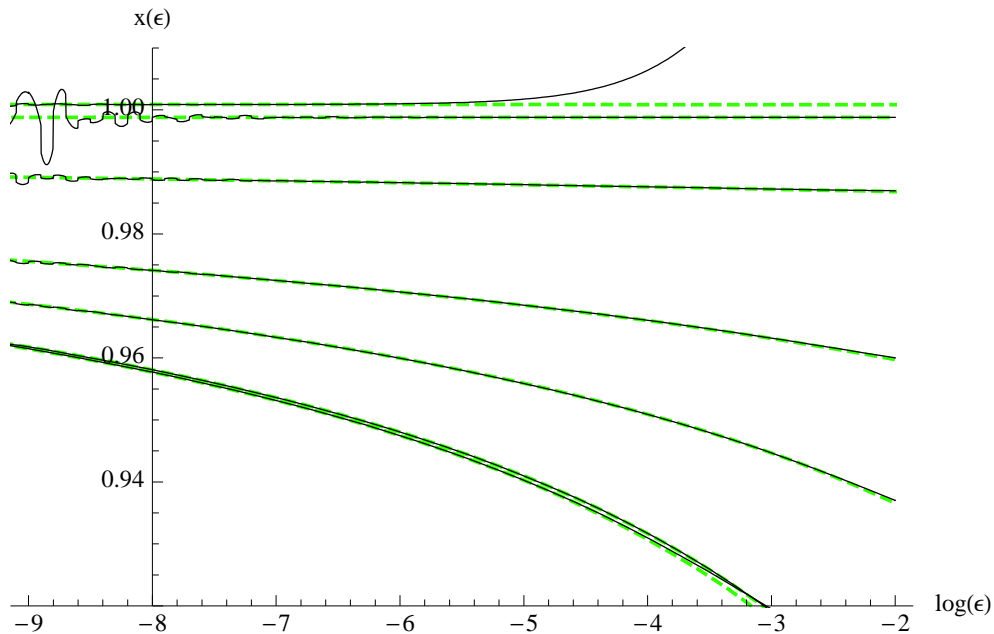


FIG. 6: Plots of the exponent $x(\epsilon)$ as defined in (63), for various values of the temperature. At zero temperature the exponent is simply 1 and all these curves should eventually limit to 1 at small enough densities. The slow running of this exponent is a consequence of the $\log \epsilon$ behavior of the chemical potential. The dashed line is a (1 parameter) fit to the numerical curve using (64).

Again we can use exact (numerical) solutions for small densities to check our analysis. The $\log \epsilon$ dependence is not easy to see, so we must push our analysis to very small densities

with a wide range of densities. Then the best way to extract the behavior is to plot the function $x(\epsilon)$ defined by,

$$x(\epsilon) = \frac{d \log(\mu_q - m_q^{(T)})}{d \log \epsilon} \quad (63)$$

$$\approx \frac{A(T) - B(T)(\log \epsilon + 1)}{A(T) - B(T) \log \epsilon} \quad (64)$$

where for the last equality we have used our derived small ϵ expression (60). We can fit this later form to the numerical result and find the ratio $A(T)/B(T)$, after which we can use the overall normalization of $\mu_q - m_q^{(T)}$ to fix $A(T)$ and $B(T)$ separately. This agreement in the form of the solution is shown in Fig. 6.

C. Behavior of $B(T)$ and $A(T)$

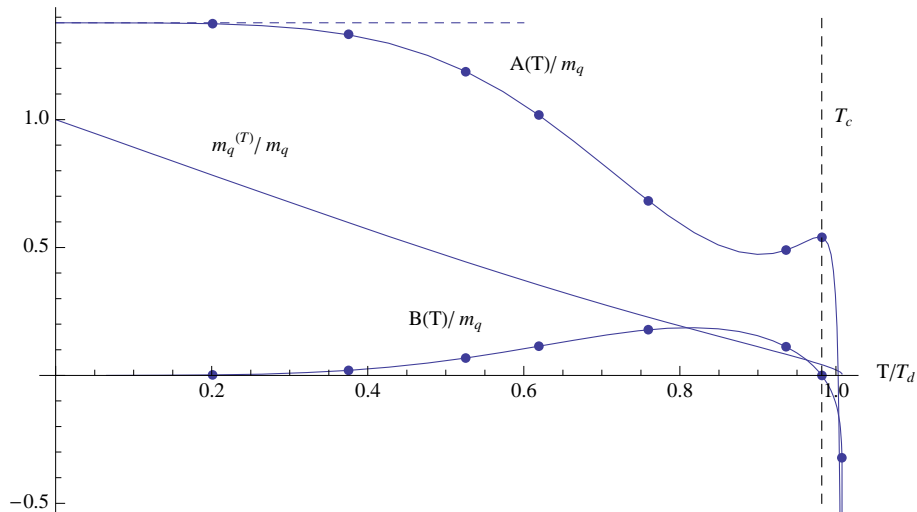


FIG. 7: The quantities in (60) are plotted as a function of T/T_d . The dots represent the values of $A(T)$ and $B(T)$ obtained through fitting the numerical results to the form of the small density expansion. The actual curves come from the results of section III (which also require numerics to calculate $A(T)$.) The consistency is gratifying.

Let us now examine the behavior of $B(T)$ and $A(T)$ as we vary T . In the $T \rightarrow 0$ (i.e. $\eta \rightarrow 0$) limit, from (61)

$$m_q(T) = m_q, \quad A(T) = m_q \frac{\kappa^3}{2}, \quad B(T) = 0 \quad (65)$$

which reduces to the correct zero temperature behavior (A4) in Appendix A. In the above equation κ is a number defined by the integral $\kappa = \int_0^\infty dx/(x^6 + 1)$. For general temperature T , the behavior of $A(T)$, $B(T)$ and $m_q^{(T)}$ are plotted in Fig. 7. Note that in obtaining Fig. 7 we have converted the dependence on η into T and also the temperature dependence of L_0 using the relations demonstrated in Fig. 3.

Note that $B(T)$ is positive at small temperature and becomes negative for

$$\eta > \eta_c, \quad \eta_c = \left(\frac{1}{3}(4 - \sqrt{7})\right)^{\frac{1}{4}}, \quad \text{i.e. } T > T_c, \quad T_c \approx .982T_d, \quad B(T_c) = 0 \quad (66)$$

Also note that $A(T)$ becomes negative at some temperature higher than T_c . Furthermore it can be shown that $A(T)$ diverges at a temperature T_m ($T_m 1.008T_d$), beyond which Minkowski embedding no longer exists; clearly our analysis does not apply since there is no zero density solution about which to perturb in ϵ .

IV. THERMODYNAMICS

From our small ϵ analysis we can now extract some important aspects of the thermodynamics of this gauge theory. We will mostly work in the grand canonical ensemble, where we fix T, μ_q and use the pressure $P(\mu_q, T)$ as the appropriate thermodynamic potential.

A. A third order phase transition for $0 < T < T_c$

As noted above $B(T) > 0$ for $0 < T < T_c$. In this case (60) may be inverted to find $\epsilon(\mu_q)$ which is then a single-valued function of μ_q for $\mu_q > m_q^{(T)}$. In other words there is only a single black hole embedding for a given fixed $\mu_q > m_q^{(T)}$. Thus for $B(T) > 0$ we conclude there is a continuous phase transition at $\mu_c = m_q^{(T)}$. For $\mu_q < m_q^{(T)}$ we have a single Minkowski embedding with $\epsilon = 0$.

Examining derivatives of the pressure on either side of $m_q^{(T)}$ one finds for $\mu_q < m_q^{(T)}$,

$$P(T, \mu) = P_0(T), \quad n_q = \frac{\partial P_0}{\partial \mu_q} = 0, \quad \frac{\partial^n P_0}{\partial \mu_q^n} = 0, \quad \text{for all } n \geq 1 \quad (67)$$

and for $\mu_q > m_q^{(T)}$, we find

$$\frac{\partial^2 P}{\partial \mu_q^2} \propto \left(\frac{\partial \mu_q}{\partial \epsilon}\right)^{-1} = \frac{1}{A - B - B \log \epsilon} \quad (68)$$

and

$$\frac{\partial^3 P}{\partial \mu_q^3} \propto -\frac{\partial^2 \mu_q}{\partial \epsilon^2} \left(\frac{\partial \mu_q}{\partial \epsilon} \right)^{-2} = \frac{B}{\epsilon} \frac{1}{(A - B - B \log \epsilon)^2} \quad (69)$$

In the limit $\epsilon \rightarrow 0$, $\frac{\partial^2 P}{\partial \mu_q^2} \rightarrow 0$ and $\frac{\partial^3 P}{\partial \mu_q^3} \rightarrow \infty$. This implies that there is a third order phase transition since the third derivative of the pressure is discontinuous across the phase boundary. Also since $\frac{\partial P^2}{\partial \mu_q^2} > 0$, the system is thermodynamically stable.

Note that exactly for $B(T) = 0$ the transition becomes second order, since (68) is then discontinuous across the phase boundary. This happens at two places, the first is the zero temperature critical point which was studied in [11]. The second is a new critical point at $(T, \mu) = (T_c, \mu_c)$ where T_c is given in (66) and $\mu_c = m_q^{(T=T_c)} \approx .0418 m_q$. We will discuss the phase structure around this point in the next subsection.

In Fig. (1) we display the phase diagram in the $\mu_q - T$ plane, where this 3rd order phase transition is the predominant feature.

B. First order phase transition for $T > T_c$

Beyond the critical point $T > T_c$ we find that $B(T)$ becomes negative. From (68) this implies that $\frac{\partial^2 P}{\partial \mu_q^2}$ becomes negative in the limit of small ϵ indicating a thermodynamic instability.

To see what happens beyond T_c , let us plot μ_q at fixed T as a function of ϵ . As indicated in the left plot of Fig. 8 the curve drops below $\mu_q = m_q^{(T)}$. Since we expect the curve will go up again for sufficiently large density, there must be at least one minimum somewhere, which we call will μ_{\min} . This minimum satisfies $\mu_{\min} < m_q^{(T)}$. That is there will be multiple black hole embeddings for a fixed $\mu_q > \mu_{\min}$ and which appear as a function of μ_q before one reaches $\mu_q = m_q^{(T)}$. This allows for the possibility of a first order phase transition from the Minkowski embedding with $\epsilon = 0$ to a black hole embedding with $\epsilon = \epsilon_d(T) \neq 0$ for some chemical potential $\mu_q = \mu_d(T)$ between $\mu_{\min} < \mu_d < m_q^{(T)}$. In this way one circumvents the thermodynamically unstable solution.

Although this discussion was quite general for $T > T_c$, we can make it more explicit by considering temperatures $|T - T_c| \ll T_c$, then the minimum and the other black hole embedding still lie at small enough values of ϵ that (60) applies with only small corrections. The left plot of Fig. 8 gives the behavior of the chemical potential as a function of quark density near T_c and the right plot of Fig. (8) demonstrates the swallow tail behavior of the

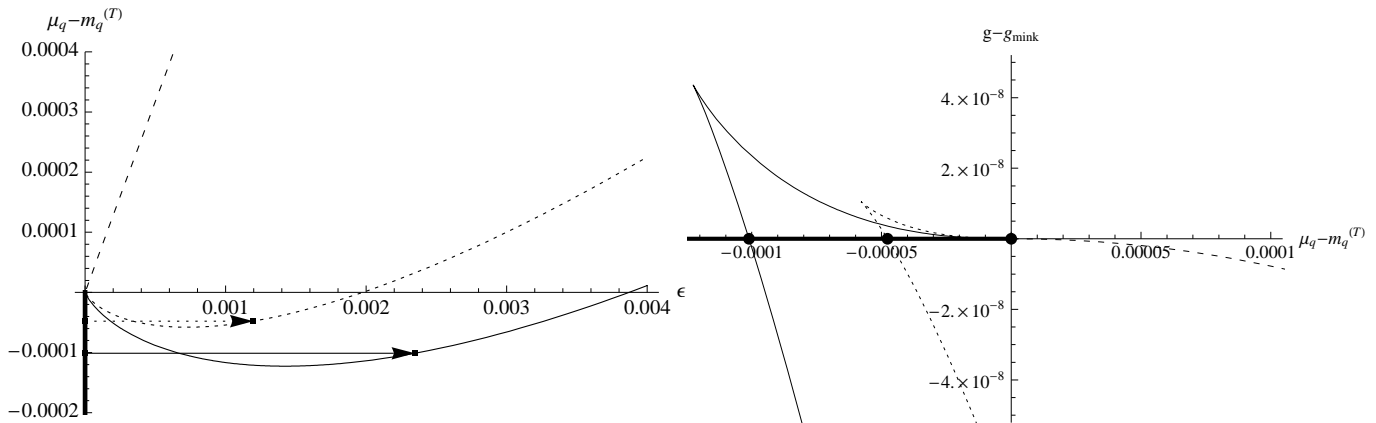


FIG. 8: (*left*) The quark chemical potential as a function of quark density, for three temperatures $T/T_d = .980, .995, .996$. The first (long dashes) is below T_c and has no minimum. For the other two we have indicated the chemical potential at which the transition occurs. (*right*) The grand potential density (related to the pressure by $P = -g$) as a function of chemical potential for the same temperatures as the left figure.

pressure for this first order transition. Using (60), the first order transition point μ_d and the discontinuity in the density ϵ_d can be expressed in terms of the functions $A(T)$ and $B(T)$ as

$$\epsilon_d(T) \approx \exp\left(\frac{A - B/2}{B}\right) \quad \mu_d(T) - m_q^{(T)} \approx \frac{1}{2}B\epsilon_d(T) \quad (70)$$

and very close to T_c we can expand $A(T)$ and $B(T)$

$$A = A_c + \mathcal{O}(T - T_c), \quad B = -B'_c(T - T_c) + \mathcal{O}(T - T_c)^2 \quad (71)$$

to find

$$\epsilon_d(T) \approx \exp\left(-\frac{A_c}{B'_c(T - T_c)}\right) = \exp(-.12T_d/(T - T_c)) \quad (72)$$

In Fig. (9) we plot ϵ_d and μ_d as functions of T near T_c using (70).

To conclude this section we note that our analysis near T_c relies on the small density behavior (60). An implicit assumption in our discussion is that various curves in the left plot of Fig. 8 does not turn back down at larger densities. While our small ϵ analysis itself does not rule out this possibility, we believe it does not happen for temperature sufficiently close to T_c from our own numerical study of embedding solutions and from the finite density analysis of [16].¹⁹ Our analysis of the first order phase transition cannot be trusted for

¹⁹ At some higher temperature, this could happen.

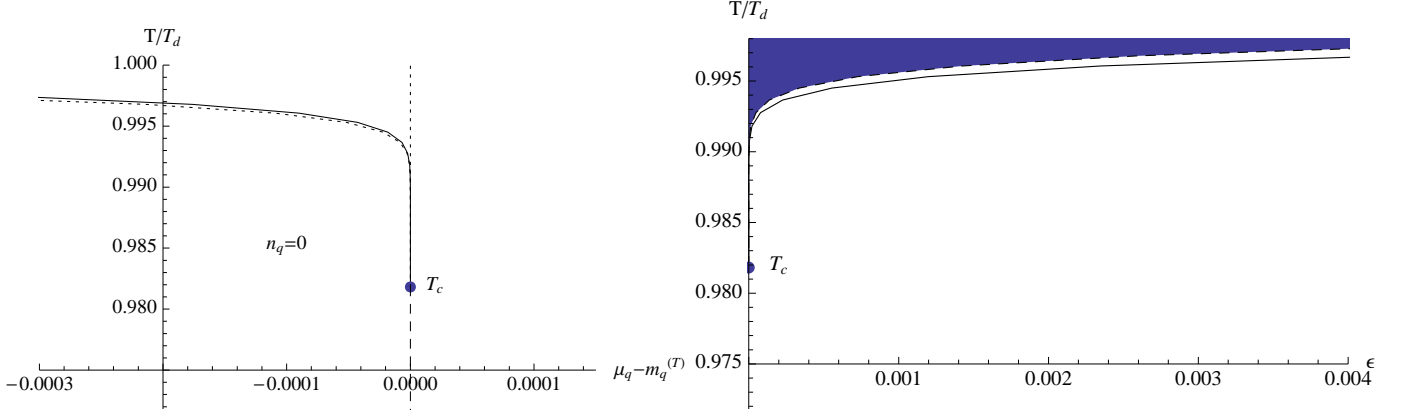


FIG. 9: (*left*) The first order phase transition line (solid) close to the critical point, in the $(\mu_q - m_q^{(T)}) - T$ plane. Also shown (dashed) is the region where multiple embeddings are available at fixed μ_q . (*right*) The behavior of $\epsilon_d(T)$ above the critical temperature. The shaded region represents the onset of a thermodynamic instability. In the canonical ensemble this region is circumvented as usual by the Maxwell construction.

temperatures too high above T_c - since then the density at the first order phase transition will lie out of the range of applicability of (60). Note that (60) is likely to break down much earlier than simply when $\epsilon \sim 1$. The reason for this is that at some temperature multiple embeddings for a fixed *density* should appear, something which our analysis has not allowed for. This is clearly the case (as discussed earlier) for zero density, where there exists a temperature $T_{bh} < T_d$ above which multiple embeddings are allowed (the original Minkowski embedding and two new black hole embeddings).²⁰ One expects this to be the case for small densities. Indeed these new embeddings will be continuous deformations of black hole embeddings away from zero density, so our starting point (Minkowski embeddings) is not good for seeing these multiple embeddings. As we will discuss later the reason for this break down is closely related to how this line of first order phase transition connects to the zero density dissociation transition.

²⁰ Note that $T_{bh} = 0.9975T_d$ is far enough away from $T_c = .982T_d$ that one can trust that multiple embeddings do not appear then.

V. CONCLUSIONS AND DISCUSSIONS

In this paper we showed that in the plane of temperature v.s. baryon chemical potential there is a critical line of third order phase transition which ends at a tricritical point after which the transition becomes first order. The critical behavior at the critical line is given by (60) which contains an intriguing logarithmic behavior. It would be interesting to have a microscopic understanding of this behavior, and more generally the structure of the whole phase diagram. In particular, it would be interesting to see whether the logarithmic behavior is related to the spiral behavior observed in [7, 20] at zero chemical potential. Below we discuss in more detail two open issues of our investigation.

A. Connection to the dissociation transition

To complete the phase diagram, we need to address whether the first order phase transition slightly above T_c discussed in sec. IV B connects to the first order phase transition along the vertical axis at $T = T_d$ and $\mu_q = 0$, and if yes, how. Note that such a conclusion is suggested by numerical work in [10] and is consistent with the numerical work in [12].

For convenience of discussion let us first briefly review some important aspects of the transition at $\mu_q = 0$. At a low temperature there is only Minkowski embedding. As one increases T to a temperature T_{bh} , two new black hole embeddings appear and when one further increases the temperature to $T_d > T_{bh} = 0.997T_d$, a first order phase transition occurs, above which one of the black hole embedding thermodynamically dominates over the Minkowski embedding. For all the embedding solutions, the baryon density is zero. Thus the discontinuity $\epsilon_d(T)$ at the phase transition is trivially zero.

We now return to the question at hand, which unfortunately our analysis for small density cannot directly answer. To see this if we were to extrapolate our analysis of the 1st order phase transition line (the solid line in the left figure of Fig. 9), we find that the line $\mu_d(T)$ crosses the $\mu_q = 0$ axis at some temperature. This temperature is slightly higher than T_d and hence would seem to give an estimate of T_d itself, subject to ϵ corrections. This small difference from T_d might not seem like a problem, and one might guess we have a nice description of the physics of the zero density dissociation transition. However it is qualitatively wrong, since we also find $\epsilon_d(T)$ grows monotonically along this line. This is

qualitatively wrong because on the axis $\mu_q = 0$, the phase transition should occur at zero density. This demonstrates that (60) must have broken down quite drastically somewhere before $\mu_d(T) = 0$ is reached.

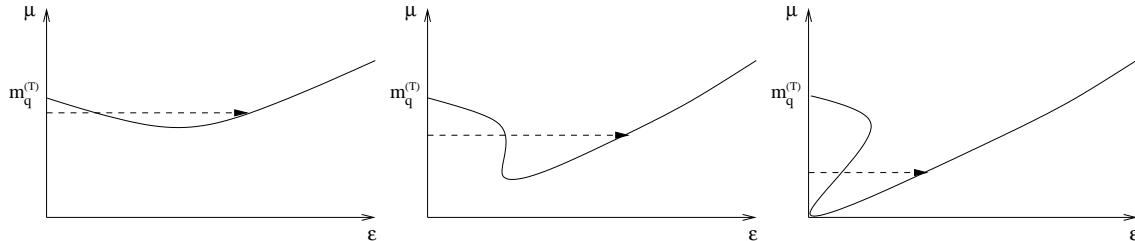


FIG. 10: The qualitative behavior of $\mu_q(\epsilon)$ at different temperatures in order for the 1st order phase transition near T_c discussed in last section to connect to the transition at $\mu_q = 0, \epsilon = 0$. Left plot: for a temperature T slightly above T_c . Middle plot: for a temperature T above T_c and below T_{bh} . Right plot: for $T \geq T_{bh}$.

We will now consider the simplest possibility, i.e. *assuming* that 1st order transition line from T_c does smoothly connect with the transition at zero μ_q . For this to happen the transition density $\epsilon_d(T)$ should first increase as we increase T from T_c (consistent with the behavior derived from (60)) and then decrease to zero as T_d is approached. In turn this implies that the minimum of the curve $\mu_q(\epsilon)$ should approach the $\epsilon = 0$ axis as the temperature is increased to $T = T_{bh}$. In Fig.10 we plot qualitatively, at different temperatures, what is required of the curve $\mu_q(\epsilon)$ for this to happen. In particular, the minimum of the curve will hit the origin $\epsilon = \mu_q = 0$, exactly at the temperature $T = T_{bh}$, where two black hole embeddings appear at zero density. For temperatures above $T > T_{bh}$ moving towards $T = T_d$ the curve $\mu_q(\epsilon)$ is similar to that at $T = T_{bh}$. However now the point at which the 1st order phase transition occurs (which we have called (μ_d, ϵ_d)) should move towards the origin. Note that plots of form of Fig. 10 were found numerically in [9].

An important feature of the last two plots Fig.10 is that when temperature is sufficiently high, μ can be multi-valued for a fixed ϵ . For $T > T_{bh}$, this is consistent with our expectation that there should be three black hole embeddings at small ϵ , two from small density perturbations of the black hole embeddings at zero density one from the small perturbation of the Minkowski embedding which we discussed earlier in this paper. We have done some preliminary study of the behavior of the $\mu - \epsilon$ plot near the origin for $T \sim T_{bh}$ from perturbing two black hole embeddings at zero density and confirmed the qualitative behavior

presented in the last two plots. But the extrapolation to the branch we studied in this paper requires studying finite density solution and that part of the curve is pure speculation at the moment. We leave the full exploration to future work.

Since, for high enough temperatures, there are multiple embeddings with different chemical potentials and the same density, if we examine the thermodynamics in the canonical ensemble, there will be an interesting set of phase transitions unrelated to the one identified above that can occur between embeddings with *different* chemical potentials, but the same density. These phase transitions are quite strange, and as discussed in [16] occur between solutions which are potential thermodynamically unstable. These transitions should involve embeddings with chemical potentials higher than that at which the 1st order phase transition in the grand canonical ensemble occurs. Hence such transitions will be hidden from the point of view of the grand canonical ensemble. Since thermodynamics should be consistent in the two different ensembles one would expect that a proper consideration of the canonical ensemble using for example, the Maxwell construction of inhomogeneous phases, should remove these differences.

B. Transition at finite λ

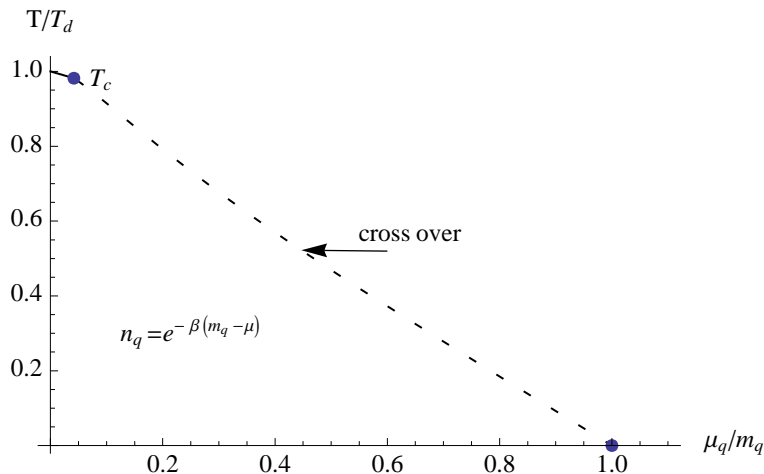


FIG. 11: Possible phase diagram at finite λ . The lower region consists of a Boltzmann gas of quarks and anti-quarks. The third order phase transition of Fig. 1 is potentially smoothed to a cross over.

Another important question is what could happen to the phase diagram at finite 't Hooft

coupling λ . At finite λ , as pointed out in [21] and commented upon earlier in [12], for any $\mu_q \neq 0$ at any finite temperature, the baryon charge density is in fact *nonzero*, given by a dilute Boltzmann gas of quarks. Thus in the phase diagram Fig. 1, the region below the critical line also has a finite density. This is of course expected for a deconfined plasma. In particular the value of quark density at the transition line should be nonzero and continuous at finite λ . This immediately raises the possibility whether the transition is smoothed into a crossover at any finite λ . To have a definite answer to this question requires summing over the instanton contributions in (32) for all n and then taking the limit $\mu_q \rightarrow m_q^{(T)}$ in the resulting expression. This is certainly beyond the scope of the current paper. In Fig 11 we plot qualitatively the structure of the phase diagram if the transition is smoothed out.

Here we mention another indirect indication that the transition might be smoothed out. In [21] we have argued that at any finite λ , in the region below the transition line in the phase diagram, the mesons have a width proportional to the sum of quark and anti-quark densities,

$$\Gamma = \frac{32\pi^3\sqrt{\lambda}}{N_c m_q^2} |\psi(\theta = 0)|^2 (n_+ + n_-) . \quad (73)$$

where $n_{\pm} \propto \exp(-(m_q^{(T)} \pm \mu_q)/T)$ and are exponentially small in $\sqrt{\lambda}$ as argued in sec.II C. $\psi(\theta = 0)$ is the meson wave function at the tip of the brane. We have also performed [22] a calculation of the meson width on the critical line from above and found at small densities exactly the same answer as (73).²¹ Note that one of the key signatures of the phase transition at zero density (in fact potentially the defining signature) is the spectrum of mesons (quark and anti-quark bound states)[19, 20]. Here we find the meson widths and thus the spectrum are continuous across the critical line indicating that the transition might be smoothed out.

Acknowledgments

We thank D. Mateos, R. Myers, K. Rajagopal, V. Kumar and T. Senthil for useful discussions. Research supported in part by the DOE under contracts #DF-FC02-94ER40818. HL is also supported in part by the A. P. Sloan Foundation and the DOE OJI program.

²¹ The meson widths at small density have also been studied numerically in [23].

APPENDIX A: THE ZERO TEMPERATURE SOLUTION AT SMALL DENSITIES

One way to motivate the scaling of the inner region $\rho = \sigma\epsilon^{1/2}$ is to look at the zero temperature solution in detail, where the exact solution is known.

This solution is:

$$y'(\rho) = \frac{c}{\sqrt{\rho^6 + \epsilon^2 - c^2}} \quad a'(\rho) = \frac{\epsilon}{c}y'(\rho) \quad (\text{A1})$$

where c is an integration constant related to the expectation of the mass operator dual to the field y on the gravity side. The boundary conditions are $y(0) = a(0) = 0$.

We can fix c in terms of the quark mass, or equivalently in terms of L . After rescaling as (23) by $L_0 = L$ the condition $y(\infty) = 1$ fixes the quark mass. Integrating (A1) one finds for c ,

$$\kappa^3 c^3 = (\epsilon^2 - c^2)$$

where κ is a number defined by the integral, $\kappa = \int_0^\infty dx/(x^6 + 1)$. For small densities the condensate c approaches ϵ as,

$$c \approx \epsilon - (\kappa/L)^3 \epsilon^2, \quad \epsilon^2 - c^2 \approx \epsilon^3 (\kappa/L)^3 \quad (\text{A2})$$

Note that by small densities we really mean $\epsilon \ll L^3$ or equivalently $n_q/(N_c\sqrt{\lambda}) \ll m_q^3$.

From (A1) it is clear the cross over scale for $y(\rho)$ between a flat Minkowski embedding and the curved solution going to the (AdS) horizon is $\rho^6 \sim \epsilon^2 - c^2$ or $\rho \sim \epsilon^{1/2}$ at small densities. This is the scaling that we set out to demonstrate.

Rescaling $\sigma = \rho/\epsilon^{1/2}$ we find the zero temperature *inner* solution becomes,

$$\frac{dY_0}{d\sigma} \approx \frac{1}{\sqrt{\sigma^6 + (\kappa)^3}} \quad (\text{A3})$$

In this limit the chemical potential to order ϵ receives contributions only from inner region with the result

$$\mu_q = \frac{L}{2\pi\alpha'} \left(1 + \frac{1}{2}\kappa^3\epsilon + \mathcal{O}(\epsilon^2) \right) \quad (\text{A4})$$

APPENDIX B: DETAILED ANALYSIS OF THE CHEMICAL POTENTIAL

In this appendix we give some details in the small ϵ -expansion of μ_q , equation (36), which we copy here for convenience

$$\mu_q = \frac{L_0}{2\pi\alpha'} \epsilon \int_{\rho_c}^{\infty} d\rho \frac{\sqrt{fq(1+y'^2)}}{\sqrt{\epsilon^2 + \rho^6 q^3}}. \quad (\text{B1})$$

Various functions in (B1) were introduced in (24). We split the above integral into those over the inner and outer regions

$$\mu_q = \int_{\rho_c}^{\rho_\Lambda} (\dots) + \int_{\rho_\Lambda}^{\infty} (\dots) \equiv \mu_{\mathcal{I}} + \mu_{\mathcal{O}} \quad (\text{B2})$$

which can then be expanded in terms of ϵ using the expansions (39), (40) of $y(\rho)$ in inner and outer regions respectively.

Let us first look at $\mu_{\mathcal{O}}$. We find that it starts with order ϵ

$$\mu_{\mathcal{O}} = \epsilon \mu_{\mathcal{O}}^{(1)} + O(\epsilon^2) \quad (\text{B3})$$

with

$$\frac{2\pi\alpha'}{L_0} \mu_{\mathcal{O}}^{(1)} = \int_{\rho_\Lambda}^{\infty} d\rho \frac{(1 - \eta^4/u^4) \sqrt{1 + y_0'^2}}{(1 + \eta^4/u^4)^2 \rho^3} \quad (\text{B4})$$

and $u^2 = \rho^2 + y_0^2(\rho)$. Using the expansion (41) of y_0 at small ρ , we find that the integral contains a quadratic and a logarithmic divergent term in the limit $\rho_\Lambda \rightarrow 0$, given by

$$\frac{2\pi\alpha'}{L_0} \mu_{\mathcal{O}}^{(1)} = \frac{1 - \eta^4}{2(1 + \eta^4)^2 \rho_\Lambda^2} - \frac{2\eta^4(3 - \eta^4 + 3\eta^8)}{(1 - \eta^4)(1 + \eta^4)^4} \log(\rho_\Lambda) + K_{\mathcal{O}} \quad (\text{B5})$$

where $K_{\mathcal{O}}$ denotes the finite part of the integral. It can be defined more precisely by

$$K_{\mathcal{O}} = \lim_{\rho_\Lambda \rightarrow 0} \left[\int_{\rho_\Lambda}^{\infty} d\rho \frac{(1 - \eta^4/u^4) \sqrt{1 + y_0'^2}}{(1 + \eta^4/u^4)^2 \rho^3} - \frac{(1 - \eta^4)}{2(1 + \eta^4)^2 \rho_\Lambda^2} - \frac{2\eta^4(3 - \eta^4 + 3\eta^8)}{(-1 + \eta^4)(1 + \eta^4)^4} \log(\rho_\Lambda) \right] \quad (\text{B6})$$

Once $y_0(\rho)$ is known numerically, $K_{\mathcal{O}}$ can be calculated numerically.

We now look at $\mu_{\mathcal{I}}$ which can be expanded as

$$\mu_{\mathcal{I}} = \mu_{\mathcal{I}}^{(0)} + \epsilon \mu_{\mathcal{I}}^{(1)} + \dots \quad (\text{B7})$$

The first term in the above has been discussed explicitly in the main text. Here we give some details for computing $\mu_{\mathcal{I}}^{(1)}$, which can be written as (derivatives are w.r.t. σ)

$$\frac{2\pi\alpha'}{L_0} \mu_{\mathcal{I}}^{(1)} = \int_{\sigma_0}^{\Lambda} d\sigma \left(M + \partial_\sigma \left(Y_1 \frac{(Y_0^4 - \eta^4)}{Y_0^2 (\eta^4 + Y_0^4)^{1/2}} \right) \right), \quad (\text{B8})$$

where

$$M = \frac{Y_0^4 - \eta^4}{2Y_0'Y_0^2\sqrt{\eta^4 + Y_0^4}} + \frac{\sigma^2\eta^4(\eta^4 + 3Y_0^4)Y_0'}{Y_0^4(\eta^4 + Y_0^4)^{3/2}} + \frac{\sigma^6(\eta^4 - Y_0^4)(\eta^4 + Y_0^4)^{5/2}Y_0'}{2Y_0^{14}} \quad (\text{B9})$$

The total derivative term in (B8) is nonzero only at the upper end and gives

$$\text{total} = \frac{\eta^8}{(1 + \eta^4)^{3/2}}\Lambda^2 + \frac{(1 - \eta^4)a_1}{\sqrt{1 + \eta^4}} + \frac{\eta^{12}(3 + \eta^4) - 14\eta^8 \log(\Lambda)}{(-1 + \eta^4)(1 + \eta^4)^4} \quad (\text{B10})$$

where we have used the expansions (48) and (49). The integration over M in (B8) is also divergent in the limit $\Lambda \rightarrow \infty$. The divergent terms can be extracted using the expansion (48) and one finds that

$$\int_{\sigma_0}^{\Lambda} d\sigma M = -\frac{\eta^8}{(1 + \eta^4)^{3/2}}\Lambda^2 - \frac{2\eta^4(3 - 8\eta^4 + 3\eta^8)}{(-1 + \eta^4)(1 + \eta^4)^4} \log(\Lambda) + M_f \quad (\text{B11})$$

where M_f denotes the finite part of the integral and can be defined more precisely as

$$M_f = \lim_{\Lambda \rightarrow \infty} \left(\int_{\sigma_0}^{\Lambda} d\sigma M + \frac{\eta^8}{(1 + \eta^4)^{3/2}}\Lambda^2 + \frac{2\eta^4(3 - 8\eta^4 + 3\eta^8)}{(-1 + \eta^4)(1 + \eta^4)^4} \log(\Lambda) \right) \quad (\text{B12})$$

Adding (B10) and (B11) together we find that the quadratic divergences in Λ cancel and

$$\begin{aligned} & \frac{2\pi\alpha'}{L_0}\mu_{\mathcal{I}}^{(1)} \\ &= \frac{2\eta^4(3 - \eta^4 + 3\eta^8)}{(1 - \eta^4)(1 + \eta^4)^4} \log(\Lambda) + \frac{7\eta^8 \log \epsilon}{(1 - \eta^4)(1 + \eta^4)^4} + \frac{1 - \eta^4}{\sqrt{1 + \eta^4}}b_1 - \frac{\eta^{12}(3 + \eta^4)}{(1 - \eta^4)(1 + \eta^4)^4} + M_f \end{aligned} \quad (\text{B13})$$

where we have used (52) and b_1 was introduced in (42). Equation (B13) gives (55) with the definition

$$K_{\mathcal{I}} \equiv \frac{1 - \eta^4}{\sqrt{1 + \eta^4}}b_1 - \frac{\eta^{12}(3 + \eta^4)}{(1 - \eta^4)(1 + \eta^4)^4} + M_f \quad (\text{B14})$$

$K_{\mathcal{I}}$ depends on the full solution and can be computed numerically.

-
- [1] J. M. Maldacena, *Adv. Theor. Math. Phys.* **2**, 231 (1998); E. Witten, *ibid.* 505 (1998); S. S. Gubser, I. R. Klebanov and A. M. Polyakov, *Phys. Lett. B* **428**, 105 (1998).
[2] A. Karch and E. Katz, *JHEP* **0206**, 043 (2002) [arXiv:hep-th/0205236].
[3] J. Erdmenger, N. Evans, I. Kirsch and E. Threlfall, arXiv:0711.4467 [hep-th].
[4] Q. J. Ejaz, T. Faulkner, H. Liu, K. Rajagopal and U. A. Wiedemann, *JHEP* **0804**, 089 (2008) [arXiv:0712.0590 [hep-th]].

- [5] K. Dusling, J. Erdmenger, M. Kaminski, F. Rust, D. Teaney and C. Young, JHEP **0810**, 098 (2008) [arXiv:0808.0957 [hep-th]].
- R. C. Myers, A. O. Starinets and R. M. Thomson, JHEP **0711**, 091 (2007) [arXiv:0706.0162 [hep-th]].
- J. Erdmenger, M. Kaminski and F. Rust, Phys. Rev. D **77**, 046005 (2008) [arXiv:0710.0334 [hep-th]].
- J. Mas, J. P. Shock, J. Tarrío and D. Zoakos, arXiv:0805.2601 [hep-th].
- D. Mateos and L. Patino, JHEP **0711**, 025 (2007) [arXiv:0709.2168 [hep-th]].
- J. Casalderrey-Solana and D. Mateos, arXiv:0806.4172 [hep-ph].
- [6] A. Karch, D. T. Son and A. O. Starinets, arXiv:0806.3796 [hep-th].
- M. Kulaxizi and A. Parnachev, Phys. Rev. D **78**, 086004 (2008) [arXiv:0808.3953 [hep-th]].
- M. Kulaxizi and A. Parnachev, arXiv:0811.2262 [hep-th].
- K. Y. Kim and I. Zahed, arXiv:0811.0184 [hep-th].
- [7] D. Mateos, R. C. Myers and R. M. Thomson, Phys. Rev. Lett. **97**, 091601 (2006) [arXiv:hep-th/0605046].
- [8] T. Albash, V. G. Filev, C. V. Johnson and A. Kundu, Phys. Rev. D **77**, 066004 (2008) [arXiv:hep-th/0605088].
- [9] S. Nakamura, Y. Seo, S. J. Sin and K. P. Yogendran, Prog. Theor. Phys. **120**, 51 (2008) [arXiv:0708.2818 [hep-th]].
- [10] K. Ghoroku, M. Ishihara and A. Nakamura, Phys. Rev. D **76**, 124006 (2007) [arXiv:0708.3706 [hep-th]].
- [11] A. Karch and A. O'Bannon, JHEP **0711**, 074 (2007) [arXiv:0709.0570 [hep-th]].
- [12] D. Mateos, S. Matsuura, R. C. Myers and R. M. Thomson, JHEP **0711**, 085 (2007) [arXiv:0709.1225 [hep-th]].
- [13] J. Babington, J. Erdmenger, N. J. Evans, Z. Guralnik and I. Kirsch, Phys. Rev. D **69**, 066007 (2004) [arXiv:hep-th/0306018].
- [14] I. Kirsch, Fortsch. Phys. **52**, 727 (2004) [arXiv:hep-th/0406274].
- [15] S. Nakamura, Y. Seo, S. J. Sin and K. P. Yogendran, arXiv:hep-th/0611021.
- [16] S. Kobayashi, D. Mateos, S. Matsuura, R. C. Myers and R. M. Thomson, JHEP **0702**, 016 (2007) [arXiv:hep-th/0611099].
- [17] J. Erdmenger, M. Kaminski, P. Kerner and F. Rust, JHEP **0811**, 031 (2008) [arXiv:0807.2663

[hep-th]].

[18] N. Horigome and Y. Tanii, *JHEP* **0701**, 072 (2007) [arXiv:hep-th/0608198].

K. Y. Kim, S. J. Sin and I. Zahed, arXiv:hep-th/0608046.

[19] C. Hoyos-Badajoz, K. Landsteiner and S. Montero, *JHEP* **0704**, 031 (2007) [arXiv:hep-th/0612169].

[20] D. Mateos, R. C. Myers and R. M. Thomson, *JHEP* **0705**, 067 (2007) [arXiv:hep-th/0701132].

[21] T. Faulkner and H. Liu, arXiv:0807.0063 [hep-th].

[22] T. Faulkner and H. Liu, to appear.

[23] R. C. Myers and A. Sinha, arXiv:0804.2168 [hep-th].